IEEE Journal of Microwaves

Received 2 January 2023; revised 14 February 2023; accepted 4 March 2023. Date of publication 3 May 2023; date of current version 7 July 2023.

Digital Object Identifier 10.1109/JMW.2023.3257122

Compact Near Field Wireless Energy Transfer Systems Using Defected Ground Structures

FILIPE FERREIRA, MAX FELDMAN, GIOVANI BULLA, VALNER BRUSAMARELLO, AND IVAN MÜLLER

Universidade Federal do Rio Grande do Sul, Porto Alegre 90040-020, Brazil

CORRESPONDING AUTHOR: Ivan Müller (e-mail: ivan.muller@ufrgs.br).

This work was supported by the Coordenação de Aperfeiçoamento de Pessoal de Nível Superior - Brasil (CAPES) - Finance Code 001.

ABSTRACT Near-Field Wireless Power Transfer systems have attracted attention for their potential applications, such as implanted medical devices, radio frequency identification, and portable electronic devices in general. In this context, a compact model for short-range NF-WPT systems operating in ISM frequency bands is proposed, employing the concept of ground plane aperture resonators or Defected Ground Structures (DGS). This technique allows the miniaturization of the resonator, which leads to the development of compact NF-WPT systems. The model proposed in this work aims at possible applications that require simultaneous energy and data transfer. This model operates in dual band in 433 MHz and 900 MHz frequency bands and makes use of overlapping circular DGS in order to shrink the resonator device and obtain high values of Figure of Merit (FoM) commonly used in this research area. The proposed model was designed using the electromagnetic analysis and built using Rogers RO4003 dielectric material. The designed dual-band DGS resonators have a total area of 11.7×10.2 mm^2 and when placed at a distance of 15 mm between transmitter and receiver, they have measured FoM values of 0.71 and 1.07 at 440 MHz and 918 MHz, respectively. The results were compared with related works found in the literature, and indicate a η_{WPT} of 40.9% and 49.2 %.

INDEX TERMS Dual-band wireless power transfer, resonant coupling, defected ground structure, dual-bandstop filter.

I. INTRODUCTION

Wireless Power Transfer (WPT) can be defined as the technology of transferring electrical energy from a source to a load, without the use of cables for interconnection between a transmitter (TX) and a receiver (RX), for instance, to charge the battery of an electronic device [1], [2]. WPT systems currently developed are mostly based on magnetic coupling and the applications of this technique include RFID tags, chargers for portable electronic devices and implanted medical devices (IMD) [3], in addition to being used in high-power systems, such as electric vehicles charging [4]. In IMD applications, WPT devices usage can result in quality of life improvements for patients, by avoiding surgical procedures to replace the batteries of implanted devices, such as pacemakers [5]. In other applications, WPT systems can be used in safety-critical environments, such as those containing explosive or corrosive atmospheres, or any place where there is a safety risk when an electrical connection is made or interrupted [2].

Techniques based on inductive or capacitive resonant coupling are the most widespread for WPT in near-field systems (NF-WPT). This type of coupling rely on resonant circuits that concentrate more energy over a defined frequency range so that the efficiency of WPT (η_{WPT}) can be improved. Due to the size of the coils and the need of a high quality factor (Q), resonant device solutions are sought to be used in small electronic devices and IMD, for example. Some WPT systems use printed spirals with surface-mounted capacitors (SMD) for greater miniaturization. Currently, many RF and microwave applications have used open ground structures (DGS, Defected Ground Structure) to implement low profile resonators. These structures are compact, making them suitable for WPT systems that have little usable area for resonator allocation.

Commercial products, especially portable devices such as smartphones, tablets and laptops employs standards such as the *Wireless Power Consortium* (WPC), *Power Matters Alliance* (PMA) and the *Alliance for Wireless Power* (A4WP)

which were developed by several companies to ensure interoperability in the use of charging platforms by devices of different brands [6].

Current literature presents several systems based on DGS resonators for a wide variety of applications such as IMD and RFID [7], [8], including multi-band WPT systems to meet applications that require power and data transfer concurrently [9], [10]. The dual-band system features the convenience of powering the receiving device while providing the data link for wireless communication. A possible application of the dual-band device is an IMD operating at 433 and 900 MHz, where energy transfer is performed at a lower frequency than data transfer, since absorption by living tissue is greater with increasing frequency. Therefore, the implanted device's power supply is guaranteed, leaving the communication channel operating at higher frequency and wider bandwidth.

DGS resonators can be designed in a variety of geometric shapes. These devices features frequency response of a band-stop filter (BSF) and WPT mostly is performed with two resonators placed facing each other [11], [12]. In addition, when applied to microstrip lines (ML) with two resonators coupled together, the microstrip is used as an open-circuit terminated *stub* to perform the impedance matching of the devices, aiming to maximize power transfer. The length of the ML is a limiting factor in the design of WPT systems at lower frequencies. The lower the operating frequency, the longer the ML, increasing the overall size of the structure. Typically, designs that implement DGS in WPT systems aim to obtain compact structures and, therefore, according to [13], these structures are generally implemented at frequencies above 100 MHz.

This work presents the EM analysis software design, prototyping and experimental validation of a device based on DGS, aiming to apply these structures in NF-WPT systems. It is proposed a dual-band DGS-based NF-WPT system operating in ISM bands. The target applications require specific frequency bands for energy and data transfer so proper frequency, power, and bandwidth can be adjusted. The measured results indicate an η_{WPT} of 40.9% and 49.2 %, and measured FoM values of 0.71 and 1.07 at a distance of 15 mm, in 433 MHz and 900 MHz bands, respectively, with devices measuring 11.7 x 10.2 mm^2.

II. DEVELOPMENT OF DGS-BASED NF-WPT

Most WPT systems employ magnetic or electrical (inductive, coils and capacitive, couplers) with or without resonance, that are not radiant [2]. Coils for WPT are usually bulky and large, and need careful manufacturing to maintain a high quality factor (Q). Therefore, to apply such components in small electronic equipment, such as IMD, can be a hard task. The use of DGS has grown over the years, in applications including band stop filters, antenna tuning, and WPT devices. Some works are found in the direct subject of this article, including the development of dual-band devices, with the aim of providing power and data communication. In the microwave frequency range, developed devices employ DGS as an element to obtain compact and low-profile structures. These features are essential to be implemented on portable devices [2], [13]. In general, performing magnetic coupling requires a resonator and a DGS structure associated with a parallel capacitor, to present a resonant circuit behavior, which leads to the use of these structures to form resonant devices in NF-WPT systems. In addition, they have a frequency response characteristic of BSF and, therefore, the power is transfered when the ground (GND) of these resonators are placed facing each other [11], [13], [2].

A NF-WPT system based on DGS is in [14], which was built with an H-shaped opening. An efficiency η_{WPT} of 85% was reached at a distance of 5 mm and FoM of 0.17 with the devices operating at 1 GHz frequency. Prior to this one, many attempts to use DGS are found applying this concept to build filters and oscillators in microwave range. Some examples are [15] and [16].

A NF-WPT system that implements DGS resonators in semi-H format based on [14], is presented in [17]. A comparison is made concerning different DGS formats, pointing out that the semi-H format has a greater inductance and consequently a greater η_{WPT} reaching 73% of η_{WPT} at a distance of 25 mm. DGS in square spiral shape of symmetrical and asymmetrical shapes are investigated in [18]. Results indicate a η_{WPT} of 88% and 78% at a distance of 50 mm and 40 mm, respectively, for the symmetrical and asymmetrical shapes.

EM simulation for designing filters using different DGS formats, have shown that Q factor is not substantially influenced by the DGS format [13]. Therefore, the area of a DGS is what guarantees a greater inductive reactance. Also, the authors indicate that DGS-based systems have a moderate η_{WPT} compared to coil-based systems.

DGS are employed to provide rectenna size reduction for RF-DC conversion in WPT systems in the 2.45 GHz band [19]. The authors state that the use of DGS is advantageous for providing tuning while reducing the size of the device. High efficiency is obtained while keeping antenna miniaturization. The control of cross-polarization in antennas is also possible by using DGS, by adding the etched slot elements in ground plane which can suppress undesired polarization an boost desired ones [20].

Simultaneous WPT is explored for power supply and data transferring by using coupled DGS resonators [21]. The design makes use of band stop filters as basement, although it works in much lower frequencies (49.6 MHz and 149 MHz) when compared whit this proposal.

The DGS technique is described as the intentional insertion of resonant openings in transmission lines such as ML, *Stripline* and coplanar waveguides. The DGS is inserted directly over the GND plane and its insertion leads to the disturbance of the current distribution in the plane, which changes the characteristics of the ML resulting in modification of the reactance [2]. Microstrip lines are popular planar transmission lines because they are easily integrated into passive

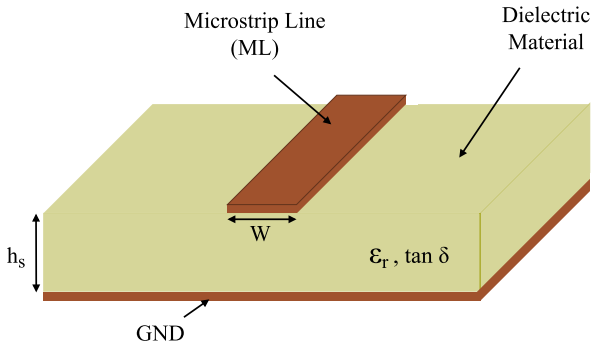

FIGURE 1. Microstrip Line geometry in an isometric view.

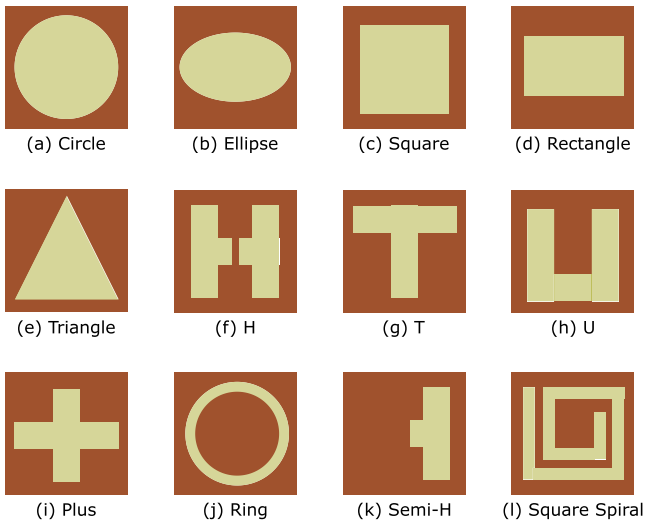

FIGURE 2. Different geometric shapes used in DGS.

and active microwave devices. In Fig. 1 the geometric structure of an ML is presented, being composed of a conductor of W width placed above a dielectric substrate that presents a relative electric permittivity (ϵ_r), loss tangent (tan δ) and a thickness (h_s) that separates it from a GND [22].

The slots printed on the GND of ML are resonant and can have a periodic or cascade structure [2]. The use of DGS allows the designer to employ different geometries to implement such structures, shown in Fig. 2.

One of the design challenges of this subject is related to the DGS equivalent circuit. Therefore, by associating a capacitor to the structure forming a resonator, the DGS-capacitor set composes a so-called quasi-concentrated device. Thus, the equivalent circuit can be modeled using LC elements, where the DGS presents an inductive reactance in a specific frequency range, intrinsically linked to its area. The physical dimensions of the DGS are critical design parameters. Different methods, such as modeling by curve fitting of scattering parameters (S), quasi-static modeling and modeling using inverters of admittance (J), are some examples [2], [23].

S-parameters obtained by EM simulation to determine the parameters of equivalent circuit and the impedances, can be extracted to adapt the equivalent circuit model. However, the frequency response of the DGS is not predictable until the solutions are optimized through studies of parametric variations. In quasi-static modeling, the equivalent circuit is derived using expressions for equivalent inductance and capacitance obtained by analysing the current returning to the ML because of disturbances caused by the DGS [23]. The method based on J inverters starts from the premise of reducing a predetermined equivalent circuit, knowing the inductance of the DGS and the measured mutual coupling (M) to a simplified equivalent which is used to determine the missing components [10], [11].

The designs carried out and discussed in this work are implemented using the S-parameters curve-fitting method. In Fig. 3 the procedures to obtain the proposed NF-WPT systems are presented in flowchart-like diagram. Initially, the dielectric material is determined, considering its electrical characteristics, such as: relative dielectric constant of the material (ϵ_r), loss tangent (tan δ), thickness of the dielectric material (h_s) and thickness of the copper layers h_{copper}. Subsequently, the DGS format is chosen and the EM simulation model of the resonator is designed as a two-port structure connecting the two ends of the ML. This device must have a frequency response characteristic of a BSF with a flat passband response (Butterworth-type response). Full-wave software EM simulations were used to analyze S-parameters of the device. If the results do not meet the desired requirements, the dimensions of the DGS and the capacitance value used to form the resonator are modified through parametric studies until they are reached. With the S-parameters in compliance with desired results, an equivalent circuit model is simulated in circuit analysis *software* using the inductive, capacitive and coupling characteristics obtained in EM simulation. Subsequently, two of the resonant devices designed to model a NF-WPT system in an EM simulation environment are used. These devices are positioned with their ground planes facing forward and separated by a distance for which the system will be optimized. The same process of checking the S-parameters is carried out until the requirements are met and then an equivalent circuit is developed to validate the designed system. Therefore, these devices are built and used as TX and RX to perform measurements of their S parameters using a vector network analyzer (VNA).

III. DUAL BAND WPT MODEL

As described before, DGS-based resonators can be designed in a variety of geometric shapes. Structurally, the DGS is basically an opening in the ground plane, in this case, a ML. The gap disturbs the current distribution in a variety of ways which leads to various frequency band rejection characteristics. Regardless of geometry, these devices exhibit a frequency response characteristic of BSF, and WPT occurs when the ground planes of two such devices are placed face-to-face. With both TX-RX device magnetically coupled, the ML is used as an open-circuit terminated *stub* to perform the impedance matching. Circular DGS with different overlapping diameters, as shown in Fig. 4 where implemented in order to obtain a structure as compact as possible.

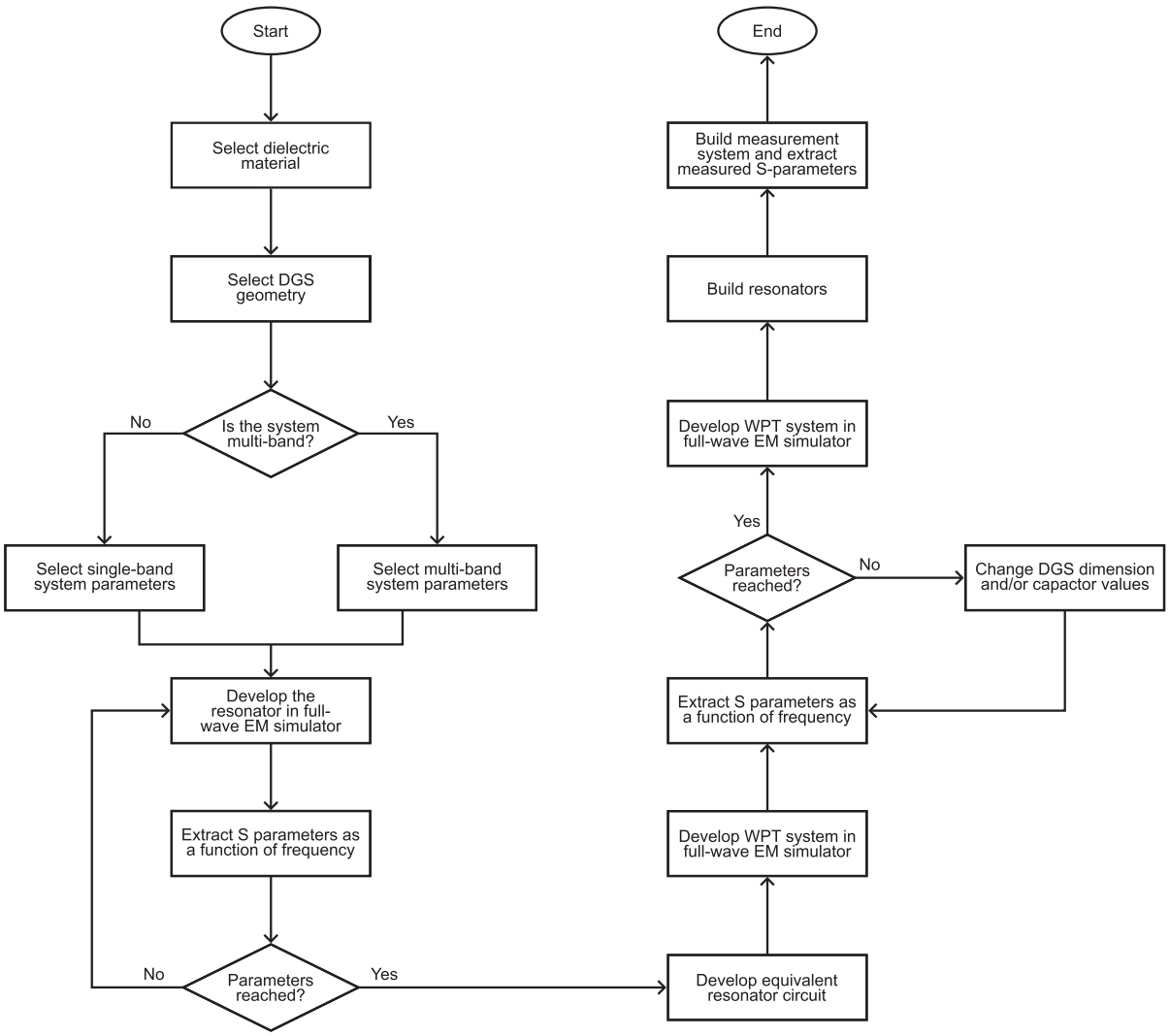

FIGURE 3. **Design methodology of a NF-WPT system based on DGS represented in a block diagram.**

The Q factor of the device is not influenced substantially by the shape of the DGS [13]. Inductive reactance of the DGS is mainly dependent of its area. The shape is chosen based on the design simplicity of the circular format. By changing the aperture diameter, one can vary the inductive reactance, which makes parametric studies via EM software faster and more efficient.

The choice of the overlapping circular shape is made taking into account that the geometric shape of the DGS does not substantially influence the Q factor. Furthermore, as the two structures get closer to each other, the coupling factor k between them increases, so the most intuitive way to increase the η_{WPT} is to increase the k between the two structures by approaching TX to RX. However, a greater proximity of TX and RX can lead to a widening of the bandpass frequency, represented in $|S_{21}|$ and to the phenomenon of division around the resonant frequency, degrading the η_{WPT}. Aiming the ISM frequency bands, 433 MHz and 900 MHz were chosen. These bands comprise, respectively, a frequency spectrum width of 433.05–434.79 MHz and 902–928 MHz [24].

The initial inductance values, corresponding to each n frequency of dual-band DGS are obtained using (1), where Z_{nn} represents the impedance seen at the corresponding DGS input. The values of Z_{nn} are obtained by simulation, where f_{rn} is the resonant frequency. Using (2), the initial values of the capacitors are calculated, and the Q factor of both DGS are obtained from (3).

$$L_n = \frac{Im\{Z_{nn}\}}{2\pi f_{rn}} \tag{1}$$

$$C_n = \frac{1}{4\pi^2 L_n f_{rn}^2} \tag{2}$$

$$Q_n = \frac{X_{DGS}}{R_{DGS}} = \frac{Im\{Z_{nn}\}}{Re\{Z_{nn}\}} \tag{3}$$

Considering the small variation of the capacitance value in these ranges, the initial design values of C_{433} and C_{900} chosen were 9.65 pF and 2.95 pF, respectively. The capacitors are placed together with the corresponding DGS in the holes C_{v1} and C_{v2}, shown in Fig. 4, where they were previously used by

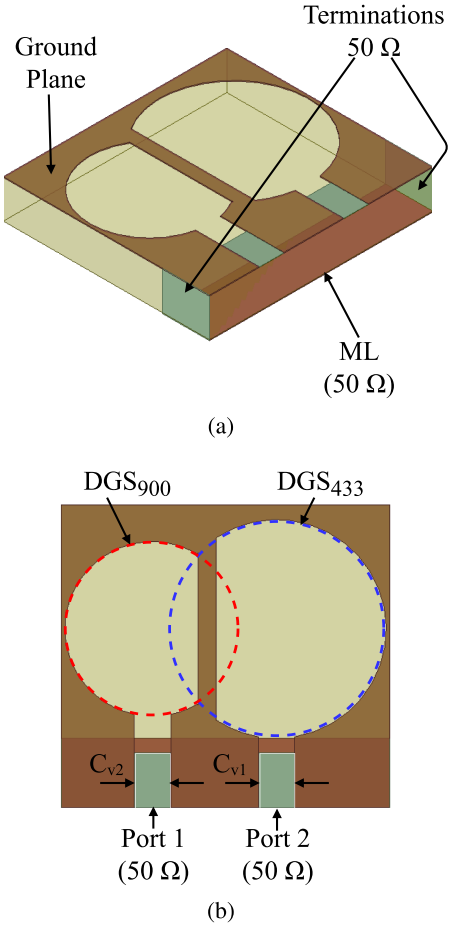

FIGURE 4. Dual band resonator in *ANSYS Electronics* EM simulation model 4(a) and superior view 4(b).

the device's source inputs to check the impedance of the DGS. C_{v1} and C_{v2} are the nomenclature chosen for the lumped ports modeled in the gaps of the DGS during EM simulation. In the first stage of the design, they are used to obtain the reactance of the DGS separately, and then, simulate the capacitors soldered in that position in the final WPT prototypes. This forms a dual-band resonant structure within the 433 MHz and 900 MHz frequency bands.

In Fig. 5, the independence between the two resonance frequencies is demonstrated by verifying the surface current density distribution (J_s). At different times, each DGS disturbs the field that propagates through the LM and resonates at a different frequency. This indicates a low level of interference between the two DGS in their frequency bands of interest. As a consequence, based on these results, the possibility of developing a dual-band NF-WPT system using the designed resonator is considered.

IV. NF-WPT SYSTEM DESIGN

In general, WPT systems require two coils or two resonators (also called antennas) operating as TX and RX. The separation distance between the TX and RX devices is a critical design parameter, as the coupling conditions are intrinsically linked

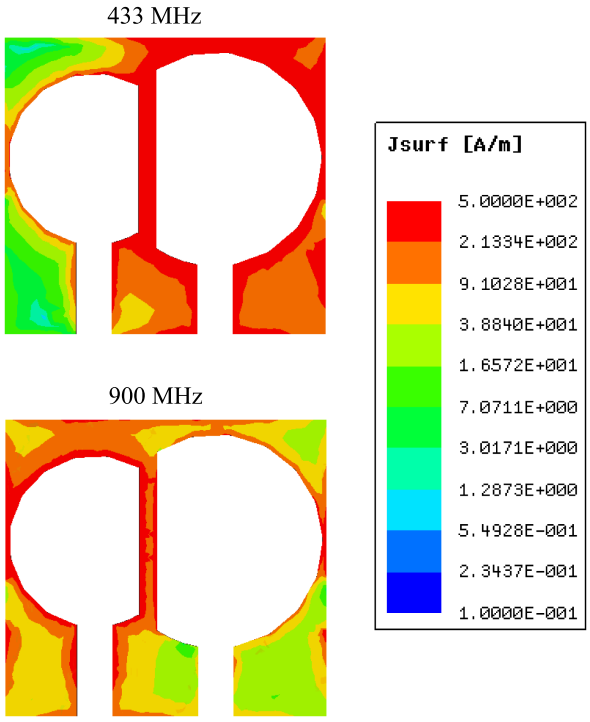

FIGURE 5. EM simulation of surface current distribution in DGS structures for each resonant frequency.

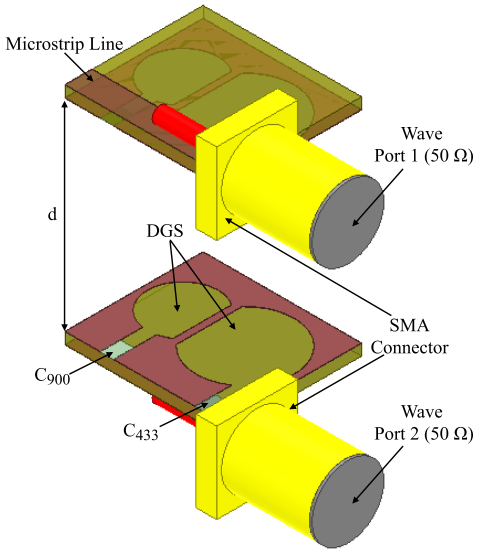

FIGURE 6. DGS-based dual-band WPT system EM simulation model.

to this distance. The smaller the distance between TX and RX, the greater the coupling between them.

In this step, through EM simulations, the S-parameters of a NF-WPT system formed by two BSF operating as resonators, with their ground planes facing each other are obtained. Fig. 6 presents the EM simulation model of the proposed WPT system. It shows two DGS devices separated by a distance d with their respective capacitors to form resonators in the 433 and 900 MHz frequency bands.

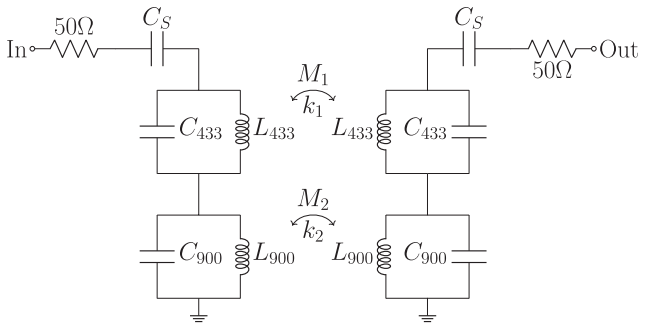

FIGURE 7. Equivalent circuit of the proposed DGS-based dual-band WPT System.

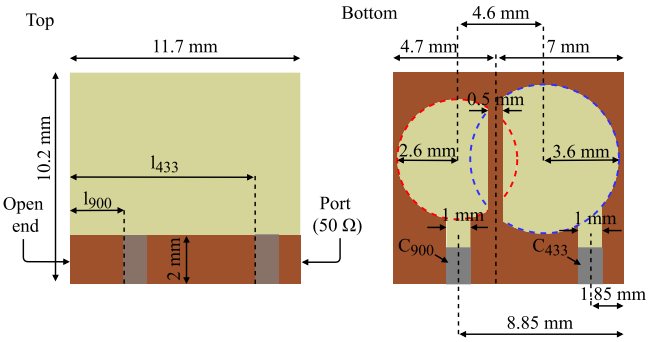

FIGURE 8. Final dimensions of the dual band resonator used to form the proposed WPT system in top and bottom views.

The two devices have identical dimensions, however they are mirrored structures so that the corresponding DGS are facing each other. Each of these devices has an excitation port forming a two-port system. Also, the circuit must be matched at 50 Ω to avoid reflections at the inputs. Therefore, the open ended ML acts as a capacitor in the circuit to perform impedance matching. (4) is used to define the capacitance of the *stub*, [22]. In this equation, β is the propagation constant and l_{st} is the length of the *stub*. The transmission line capacitance is estimated by neglecting edge effects.

$$C_S = \frac{1}{2\pi f_r Z_0} \tan(\beta l_{st}) \tag{4}$$

The equivalent circuit of this system is shown in Fig. 7, where L_{433} and L_{900} represent the inductances of the DGS resonators and C_{433} and C_{900} are the capacitors used to form the resonators in the corresponding frequency ranges. The ML capacitance is represented by C_s. Furthermore, M_1 and M_2 represent the mutual inductances and k_1 and k_2 the magnetic coupling coefficients, respectively, in the 433 and 900 MHz bands. Their values are directly influenced by the distance between the resonators and are obtained by (5) and (6) which take into account the Z-parameters of the proposed system (see Fig. 7).

$$M_1 = \frac{Im\{Z_{21}\}}{2\pi f_{433}} \quad \text{and} \quad M_2 = \frac{Im\{Z_{21}\}}{2\pi f_{900}} \tag{5}$$

$$k_1 = \frac{M_1}{L_{433}} \quad \text{and} \quad k_2 = \frac{M_2}{L_{900}} \tag{6}$$

The *stub* has width W so that the ML has an impedance of 50 Ω and its length is used to perform the impedance matching of the devices. For this, in addition to the length of the ML, both holes where the capacitors are positioned are shifted along the length of the ML. This is accomplished through parametric variations of dimensions in an EM simulation environment. The resonant device with its final dimensions is shown in Fig. 8.

For the calculation of C_s value, which represents the stub in the circuit model, β is taken into account, which is calculated from (7). The phase constant of a transmission line, β, is measured in rad/m. In this article, β_n refers to the phase constants considering the length of the microstrip line, positioned in the layer below the ground plane aperture for each DGS. The term n generalizes β with different values for the 433 or 900 MHz bands. λ_g is the guided wavelength and is dependent on the effective dielectric constant ϵ_{ef} (8). As a ML, ϵ_{ef} can be calculated using (9) [22], where h_s represents the thickness of the dielectric layer of the material and W the width of the ML. This parameter is estimated neglecting the effect of the position of the microstrip line.

TABLE 1. Physical and Electrical Characteristics of Rogers RO4003 Dielectric Material

Characteristic	Value
ϵ_r	3.55
$\tan\ \delta$	0.0027
h_s	0.813 mm
h_{copper}	0.35 μm

$$\beta_n = \frac{2\pi}{\lambda_g} \tag{7}$$

$$\lambda_g = \frac{c}{f_r\sqrt{\epsilon_{ef}}} \tag{8}$$

$$\epsilon_{ef} = \frac{\epsilon_r + 1}{2} + \frac{\epsilon_r - 1}{2}\frac{1}{\sqrt{1 + 12h_s/W}} \tag{9}$$

The dielectric substrate used in this design is Rogers RO4003. Its physical and electric characteristics are shown in Table 1. With these parameters, the values of the missing components of the equivalent circuit are determined. The S-parameters of dual band WPT system are optimized for a distance of 15 mm and for the highest possible value of FoM. As it is a symmetric and reciprocal structure, $|S_{21}| = |S_{12}|$ and $|S_{11}| = |S_{22}|$. Figs. 9 and 10 presents simulated results for $|S_{11}|$ and $|S_{21}|$, respectively, whose results indicate a good agreement between the simulated dual band WPT system in EM and circuit approach. The components values used for circuit simulation are presented in Table 2.

In order to perform the circuit analysis of the proposed dual-band WPT system model, the mutual inductance M values are extracted by means of EM analysis. Figs. 11 and 12 show the values of M simulated in the 433 and 900 MHz bands. By applying these values to (6) it is possible to calculate the k factor of this system, presented in Table 2 together

TABLE 2. Parameters for Analysis of the Equivalent Circuit of the Proposed Dual Band System

f_n	L_n	C_n	C_s	M_n	k_n	Q_n	β_n	l_n (mm)
433.26 MHz	13.90 nH	8.90 pF	0.90 pF	0.27 nH	0.019	304	15.16 rad/m	8.1 mm
916.58 MHz	10.20 nH	3.00 pF	0.23 pF	0.22 nH	0.021	308	32.03 rad/m	2.1 mm

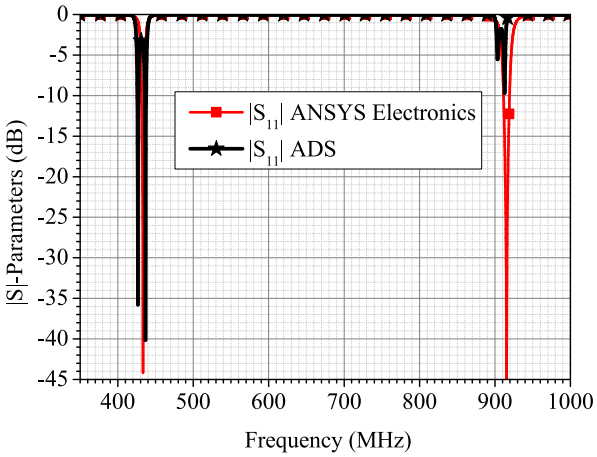

FIGURE 9. Simulated S_{11}-parameters of the NF-WPT system in the EM and circuit analysis software.

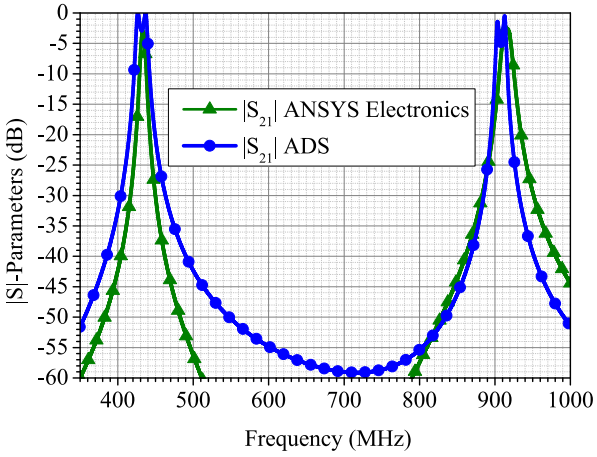

FIGURE 10. Simulated S_{21}-parameters of the NF-WPT system proposed in the EM and circuit analysis software.

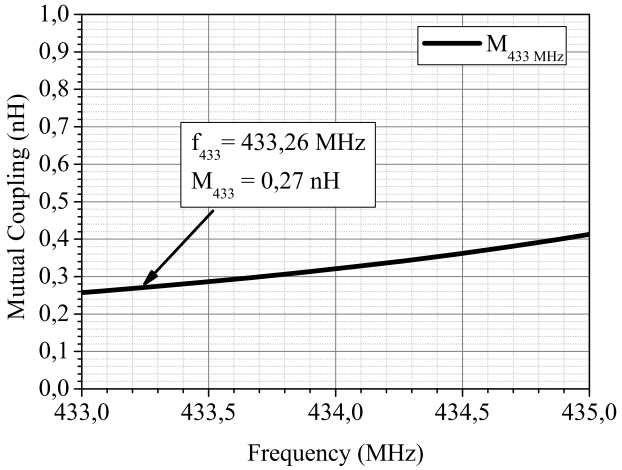

FIGURE 11. Simulated mutual coupling of the WPT system in the 433 MHz band.

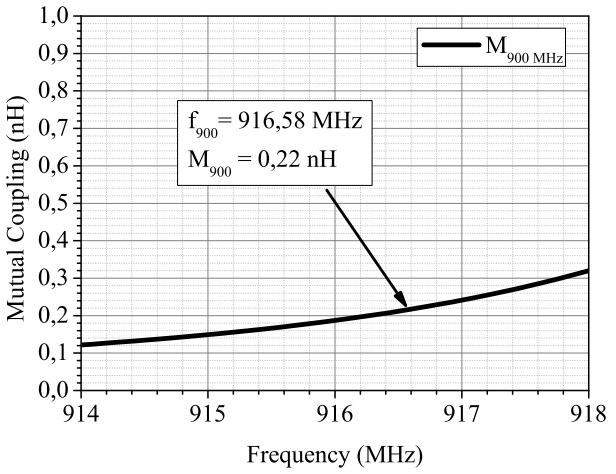

FIGURE 12. Simulated mutual coupling of the WPT system in the 900 MHz band.

with the other parameters necessary to perform the circuit analysis.

To calculate η_{WPT} and the FoM of the WPT systems, (10) and (11) are used [11], [25]. In (11) the term $A_{resonator}$ refers to the physical area of the resonator. In dual band cases, the area of the DGS and the edges of the ground plane corresponding to the resonator of each frequency band are considered. Therefore, according to Fig. 8 the area corresponding to the resonators in the 433 MHz and 900 MHz bands are 7 × 10.2 mm^2 and 4.7 × 10 mm^2, respectively. Considering the results obtained through simulation in an EM environment, the best results for $|S_{21}|$ are −3.08 dB and −2.52 dB and for $|S_{11}|$ −42. 68 dB and −46.61 dB at 433.26 MHz and 916.58 MHz. These results consider the distance between TX and RX of 15 mm for which the WPT system is optimized and can be better visualized in Figs. 19 and 20. As a consequence, $\eta_{433} = 49.21\%$ and $\eta_{433} = 55.97\%$, which lead to FoM values of 0.87 and 1.21, respectively.

$$\eta_{WPT} = \frac{|S_{21}|^2}{1 - |S_{11}|^2} \tag{10}$$

$$FoM = \eta_{WPT} \frac{d}{\sqrt{A_{ressonador}}} \tag{11}$$

In an EM simulation environment, a parametric study of the η_{WPT} and FoM as a function of the distance between TX and RX is carried out and is shown in Figs. 13 and 14. The results show that at a distance of 8 mm there is a maximum η_{WPT} of 72% at 433.26 MHz and 75.6% at 916.58 MHz. However, the best FoM values are obtained at a distance between 14

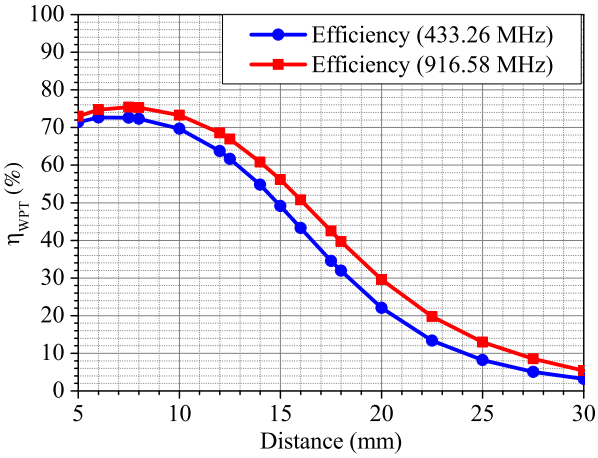

FIGURE 13. Graphs of the simulated η_{WPT} as a function of the distance between the TX and RX resonators at 433 MHz and 900 MHz.

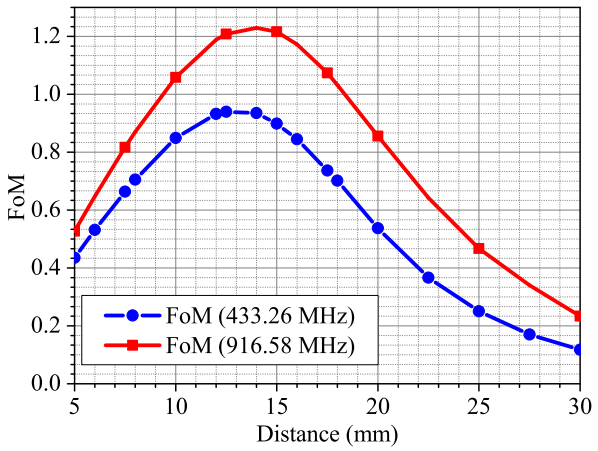

FIGURE 14. Graphs of the simulated FoM as a function of the distance between the TX and RX resonators at 433 MHz and 900 MHz.

and 15 mm for both frequency bands. The best FoM values are 0.94 and 1.23 at a distance of 14 mm, respectively at the frequencies of 433.26 MHz and 916.58 MHz.

Equation (10) is used to obtain the WPT efficiency and takes into account only the parameters $|S_{11}|$ and $|S_{21}|$. It is widely used in related articles, where they present DGS structures to form WPT systems. In this way, the WPT efficiency is measured considering the energy coupled to the input port 1 and effectively delivered to the transmitting DGS in relation to the energy measured at the output of the WPT system, disregarding the impedance matching at the receiving DGS input. Thus, the measurement of $|S_{22}|$ parameter was not carried out in the measurement tests of this proposed WPT system.

V. DGS PROTOTYPES AND MEASUREMENT ANALYSIS

Two DGS-based prototypes that make up the dual-band WPT system are built and shown in Fig. 15, and the measurements with WPT system are performed using a vector network analyzer (VNA). The equipment is the *FieldFox Keysight* model N9912 A and the measurement configuration is shown in Fig. 16, which also shows the measured parameter $|S_{21}|$. In

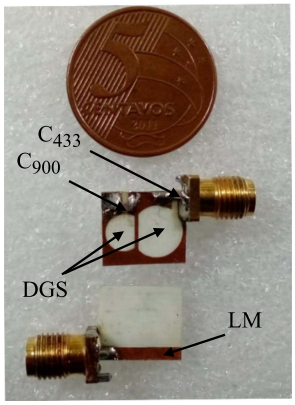

FIGURE 15. Built-in dual-band DGS-based resonator.

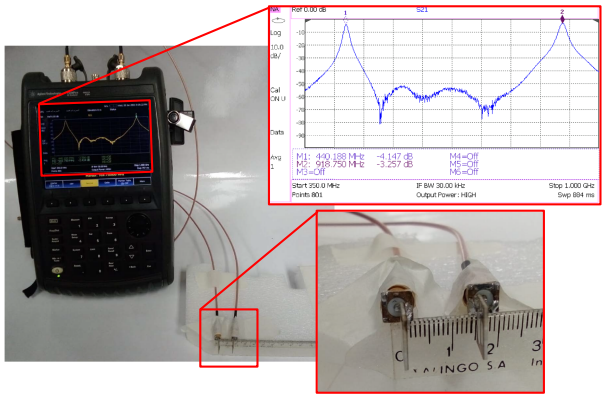

FIGURE 16. Measurement image of the proposed NF-WPT system with 15 mm distance between TX and RX.

this configuration, a ruler fixed on a styrofoam sheet is used as a measuring apparatus. Cables and devices are fixed using adhesive tape, forcing them to maintain a distance of 15 mm between TX and RX.

Capacitance values are optimized through EM simulation to obtain resonances within the 433 and 900 MHz bands, whose values are 8.9 pF and 3 pF respectively. However, because of practical aspects, SMD capacitors soldered into the devices are 8.2 pF and 3 pF, thus, 433 MHz band presents a frequency shift of approximately 6.92 MHz, resulting at 440.188 MHz. Also, Fig. 16 shows that at this frequency the value of $|S_{21}|$ is −4.147 dB, representing degradation of 1.397 dB in relation to the values obtained in EM simulation. The best measured result in the 900 MHz band is obtained at the frequency of 918.75 MHz. Despite the deviation of 2.17 MHz, the resonance remained within the ISM range of 900 MHz. As in the 433 MHz band, there is also a degradation of $|S_{21}|$, measured 0.957 dB. These degradation is caused by misalignment between TX and RX resonators.

It is possible to adjust the resonant frequency by varying only the opening of the DGS, considering a known capacitance value. However, as there is a capacitance variation within the tolerance of the SMD device, a parametric study was carried out to estimate the sensitivity of the frequency deviation. This variation is particularly noticeable in the 433 MHz ISM band range, because of its narrow frequency

TABLE 3. Summary Table - 433 MHz

Parameter	Simulation	Experimental
Frequency	433.26 MHz	440.188 MHz
S_{11}	-44.38 dB	-14.194 dB
S_{12}	-3.04 dB	-4.147 dB
Efficiency	49.21%	40.01%
FoM	0.8735	0.7102

TABLE 4. Summary Table - 915 MHz

Parameter	Simulation	Experimental
Frequency	916.58 MHz	918.750 MHz
S_{11}	-46.61 dB	-12.930 dB
S_{12}	-2.52 dB	-3.257 dB
Efficiency	55.98%	49.77%
FoM	1.2127	1.0783

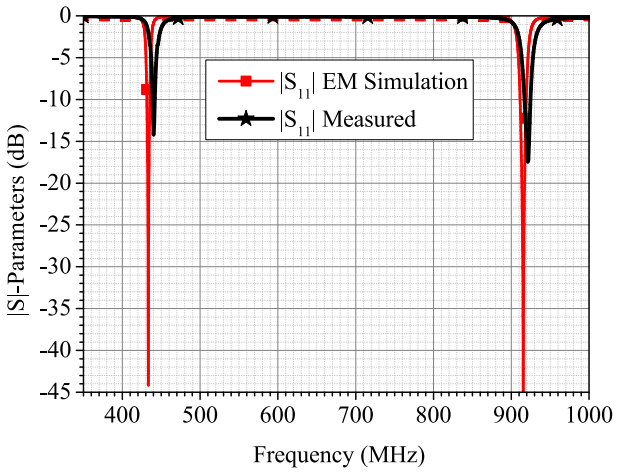

FIGURE 17. Measured and simulated S_{11}-parameters of the proposed NF-WPT system with a distance of 15 mm between TX and RX.

band (1.74 MHz of 433.05 MHz center frequency). Fig. 22 shows a +-0.2 pF of variation representing a shift of approximately 8 MHz in $|S_{21}|$.

The measurements results are compared with those obtained in EM simulation (Figs. 17 and 18). Figs. 19 and 20 show the graphs of $|S_{11}|$ and $|S_{21}|$ measured and simulated in the specific ranges. In both graphs, $|S_{11}|$ degraded in relation to the simulated one. These degradation lead to a lower η_{WPT} which is shown in Fig. 21. At 440.18 MHz frequency, a η_{WPT} of 40.9% is obtained. Comparing it with the best simulated result, at 433.26 MHz, it is concluded that there is a decrease of 7.85%. For the 900 MHz band the best measured η_{WPT}, at 918.75 MHz, is 49.2%, 7.16% below the simulated value. Despite the decrease of η_{WPT}, FoM values remained high. With values of 0.71 and 1.07, considering the frequencies of 440.188 MHz and 918.75 MHz, respectively. In the analysis of the degradation, the impedance matching system of the DGS device is designed on the EM simulation model of the WPT system, where TX and RX are face-to-face, varying the length of the microstrip line in order to optimize the system for the designed distance (15 mm). As the positioning of the

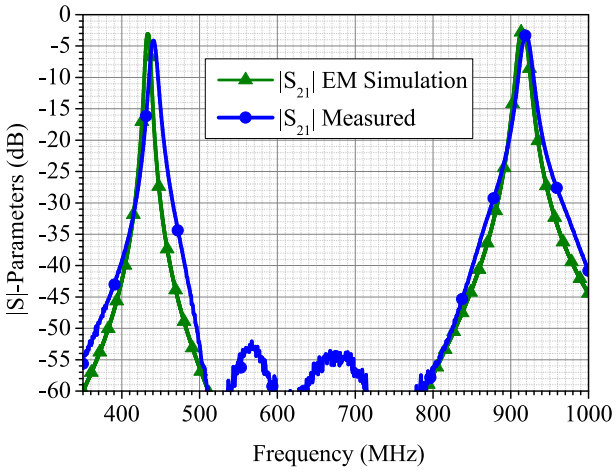

FIGURE 18. Measured and simulated S_{21}-parameters of the proposed NF-WPT system with a distance of 15 mm between TX and RX.

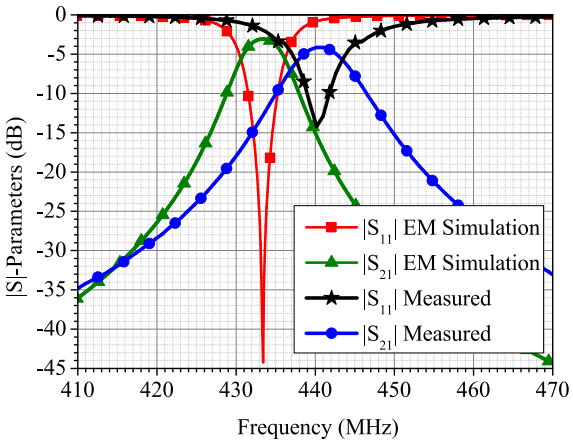

FIGURE 19. Measured and simulated S-parameters of the proposed NF-WPT system with a distance of 15 mm between TX and RX in the range of 433 MHz.

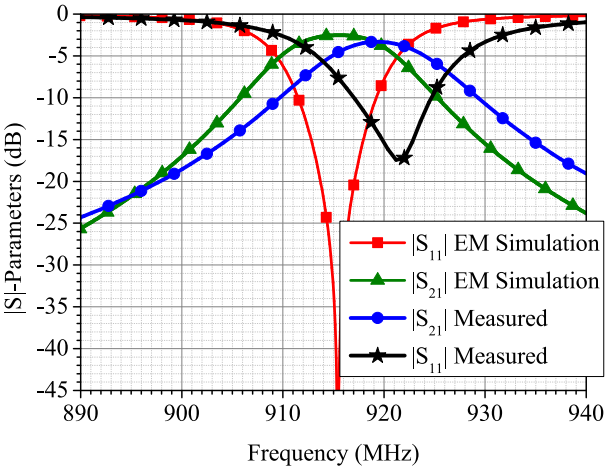

FIGURE 20. Measured and simulated S-parameters of the proposed NF-WPT system with a distance of 15 mm between TX and RX. in the 900 MHz band.

TABLE 5. Comparison of DGS-Based Dual-Band WPT Systems

Proposal	A(mm)	d(mm)	f_0(MHz)	η_{WPT}(%)	FoM
Tahar et al. [11]	30 x 15	16	300 / 700	71 / 72	0.76 / 0.77
Saad et al. [10]	44.9	10	470 / 730	52.3 / 63.7	0,78 / 0,96
Dautov, Gupta and Hashmi [25]	18 x 18	15	433 e 900	77 / 81	0.84 / 0.96
Barakat et al. [26]	30 x 30	6	50 / 100	91.2 / 79.4	0.274 / 0.238
Atallah et al. [27]	20 x 20	14	280 / 490	78 / 76	0.78 / 0.76
This work	11.7 x 10.2	15	440.188 / 918.75	40.9 / 49.2	0.71 / 1.07

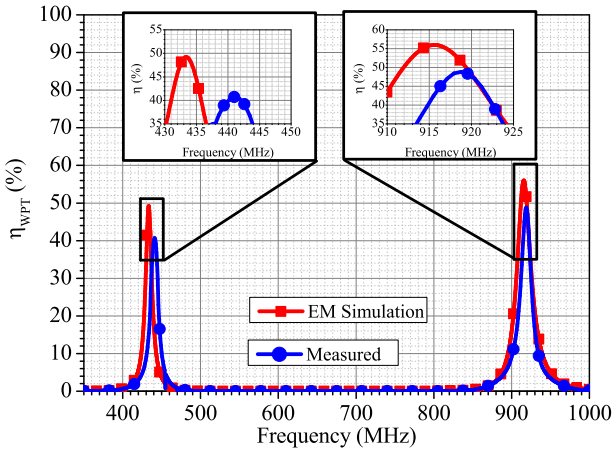

FIGURE 21. η_{WPT} **simulated and measured as a function of frequency.**

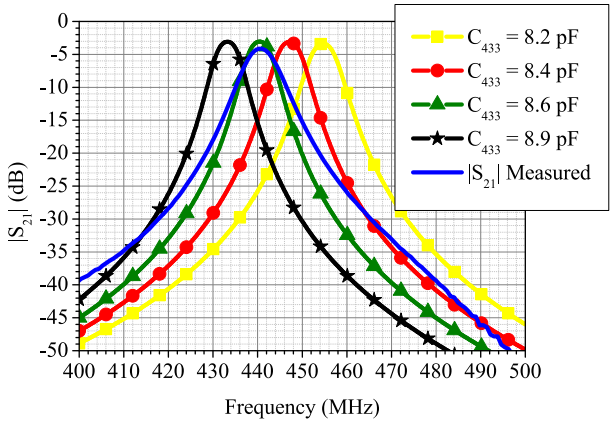

FIGURE 22. EM simulation results ranging from the capacitive value of C_{433} within the tolerance of the SMD capacitor used.

devices is changed, an impedance mismatch is caused, resulting in a degradation in the efficiency of energy transfer. In the measurement tests of the WPT system, the apparatus used to position the prototypes lacks of accuracy in the positioning of devices, so the degradation of S parameters occurs.

The frequency deviation in the 433 MHz range is caused by the use of a capacitor with a different value than the one simulated, more specifically 0.7 pF lower than the ideal value. This capacitor presents a tolerance of ±0.5 pF and Fig. 22 shows the graphs of $|S_{21}|$ simulated for values of C_{433} within this tolerance range. It can be seen that with a value of 8.6 pF there is an agreement between simulated and measured $|S_{21}|$.

Tables 3 and 4 show simulated and experimental results, for both 433 and 915 MHz frequency ranges.

Table 5 presents comparison with other DGS dual band WPT systems. The results of [25] report the same frequency ranges and distance between TX and RX, but using DGS in square format. Although the results of η_{WPT} and FoM are better in the 433 MHz band, it has a larger resonator size and FoM value in the 900 MHz frequency band, lower than that obtained with the model proposed in this work. In addition, even with a lower η_{WPT}, the developed prototype has a more compact size and higher FoM values considering frequency ranges close to 900 MHz.

VI. CONCLUSION

In this work, a NF-WPT with DGS was designed, simulated, built, and the results evaluated. A dual-band system operating in ISM bands was presented, targeting applications that require energy and data transfer simultaneously. The proposed DGS features a geometry of overlapping circles aiming at a compact device, while keeping the same level of η_{WPT} in both frequency bands. Although the proposed devices presented smaller measured η_{WPT} than those from the related works, it was possible to obtain structures with reduced dimensions with the method presented in this work.

The dual band system was optimized so that at a 15 mm distance, it presented high FoM values. Even though the measured η_{WPT} have suffered degradation due to misalignment, the value of FoM in the frequency of 440.188 MHz can be considered compatible with the values obtained in works that implement systems in similar frequencies. In addition, the use of commercial capacitors led to a frequency deviation of 6.92 MHz, causing the designed system to operate outside the ISM range of 433 MHz. However, at 918.75 MHz frequency, even with degradation, the FoM value remained high when compared to similar works operating in the same frequency range. The observed degradation may be due to the low precision in the alignment between the TX and RX resonators caused by mechanical inaccuracies in the measuring apparatus. Still, the designed and built dual-band resonator features overall dimensions of 11.7 × 10.2 mm^2. In the carried out research, no devices based on DGS used in NF-WPT systems presenting similar dimensions were found, suggesting the contribution of this work in the development of the state of the art.

REFERENCES

[1] T. Imura, *Wireless Power Transfer: Using Magnetic and Electric Resonance Coupling Techniques*. Singapore: Springer, 2020. [Online]. Available: http://link.springer.com/10.1007/978-981-15-4580-1

[2] S. Hekal, A. Allam, A. B. Abdel-Rahman, and R. K. Pokharel, *Compact Size Wireless Power Transfer Using Defected Ground Structures*. Berlin, Germany: Springer, 2019.
[3] T. Sun, X. Xie, and Z. Wang, *Wireless Power Transfer for Medical Microsystems*, vol. 9781461477. Berlin, Germany: Springer, 2013.
[4] C. T. Rim and C. Mi, *Wireless Power Transfer for Electric Vehicles and Mobile Devices*. New York, NY, USA: Wiley, 2017.
[5] G. Yilmaz and C. Dehollain, *Wireless Power Transfer and Data Communication for Neural Implants* (Analog Circuits and Signal Processing Series). Berlin, Germany: Springer International Publishing, 2017. [Online]. Available: http://link.springer.com/10.1007/978-3-319-49337-4
[6] Y. Lu and W.-H. Ki, *CMOS Integrated Circuit Design for Wireless Power Transfer*. Berlin, Germany: Springer, 2018. [Online]. Available: http://link.springer.com/10.1007/978-981-10-2615-7
[7] S. Malhotra, S. Verma, V. Bohara, and M. Hashmi, "Dual-band WPT system using semi-H DGS for biomedical applications," in *Proc. IEEE Asia-Pacific Microw. Conf.*, 2019, pp. 720–722.
[8] S. Malhotra and M. Hashmi, "Near-field WPT using defected ground structures for UHF RFID applications," in *Proc. IEEE Int. Conf. RFID Technol. Appl.*, 2019, pp. 16–21.
[9] F. Tahar, S. Chalise, K. Yoshitomi, A. Barakat, and R. K. Pokharel, "Compact dual-band wireless power transfer using overlapped single loop defected ground structure," in *Proc. IEEE Wireless Power Transfer Conf.*, 2018, pp. 1–4.
[10] M. R. Saad, F. Tahar, S. Chalise, A. Barakat, K. Yoshitomi, and R. K. Pokharel, "High FOM dual band wireless power transfer using bow-tie defected ground structure resonators," in *Proc. IEEE Wireless Power Transfer Conf.*, 2018, pp. 1–4.
[11] F. Tahar, A. Barakat, R. Saad, K. Yoshitomi, and R. K. Pokharel, "Dual-band defected ground structures wireless power transfer system with independent external and inter-resonator coupling," *IEEE Trans. Circuits Syst. II, Exp. Briefs*, vol. 64, no. 12, pp. 1372–1376, Dec. 2017.
[12] S. Verma, D. Rano, M. Hashmi, and V. Bohara, "A high Q dual E-shaped defected ground structure for wireless power transfer applications," in *Proc. Asia-Pacific Microw. Conf.*, 2018, pp. 1435–1437.
[13] K. Dautov, M. Hashmi, G. Nauryzbayev, and N. Nasimuddin, "Recent advancements in defected ground structure-based near-field wireless power transfer systems," *IEEE Access*, vol. 8, pp. 81298–81309, 2020.
[14] S. Hekal and A. B. Abdel-Rahman, "New compact design for short range wireless power transmission at 1Ghz using H-slot resonators," in *Proc. 9th Eur. Conf. Antennas Propag.*, 2015, pp. 1–5.
[15] Y. Zhu, X. Zhang, C. Li, F. Li, and G. Fang, "Novel compact meander-slot DGS with high quality factor," *Microw. Opt. Technol. Lett.*, vol. 50, no. 12, pp. 3164–3169, 2008.
[16] J. Jung, D.-J. Woo, C. S. Cho, and T.-K. Lee, "Power enhancement of microwave oscillator using a high-Q spiral-shaped DGS resonator," in *Proc. Asia-Pacific Microw. Conf.*, 2006, pp. 635–640.
[17] S. Hekal, A. B. Abdel-Rahman, H. Jia, A. Allam, A. Barakat, and R. K. Pokharel, "A novel technique for compact size wireless power transfer applications using defected ground structures," *IEEE Trans. Microw. Theory Techn.*, vol. 65, no. 2, pp. 591–599, Feb. 2017.
[18] S. Hekal, A. B. Abdel-Rahman, A. Allam, A. Barakat, H. Jia, and R. K. Pokharel, "Asymmetric strongly coupled printed resonators for wireless charging applications," in *Proc. IEEE 17th Annu. Wireless Microw. Technol. Conf.*, 2016, pp. 1–5.
[19] X. Lou and G.-M. Yang, "A dual linearly polarized rectenna using defected ground structure for wireless power transmission," *IEEE Microw. Wireless Compon. Lett.*, vol. 28, no. 9, pp. 828–830, Sep. 2018.
[20] Y. Zhang, Z. Han, S. Shen, C.-Y. Chiu, and R. Murch, "Polarization enhancement of microstrip antennas by asymmetric and symmetric grid defected ground structures," *IEEE Open J. Antennas Propag.*, vol. 1, pp. 215–223, 2020.
[21] A. Barakat, S. Alshhawy, K. Yoshitomi, and R. K. Pokharel, "Simultaneous wireless power and information transfer using coupled co-existing defected ground structure resonators," *IEEE Trans. Circuits Syst. II, Exp. Briefs*, vol. 68, no. 2, pp. 632–636, Feb. 2021.
[22] D. M. Pozar, *Microwave Engineering*. New York, NY, USA: Wiley, 2011.
[23] N. C. Karmakar, S. M. Roy, and I. Balbin, "Quasi-static modeling of defected ground structure," *IEEE Trans. Microw. Theory Techn.*, vol. 54, no. 5, pp. 2160–2168, May 2006.
[24] International Telecommunication Union, *Radio Regulations Articles*. Geneva, Switzerland: ITU, 2020. [Online]. Available: https://search.itu.int/history/HistoryDigitalCollectionDocLibrary/1.44.48.en.101.pdf
[25] K. Dautov, R. Gupta, and M. Hashmi, "A performance enhanced dual-band wireless power transfer system for practical ISM bands," in *Proc. Asia-Pacific Microw. Conf.*, 2019, pp. 1259–1261.
[26] A. Barakat, R. K. Pokharel, S. Alshhawy, K. Yoshitomi, and S. Kawasaki, "High isolation simultaneous wireless power and information transfer system using coexisting DGS resonators and figure-8 inductors," in *Proc. IEEE/MTT-S Int. Microw. Symp.*, 2020, pp. 1172–1175.
[27] H. A. Atallah, R. Hussein, and A. B. Abdel-Rahman, "Compact coupled resonators for small size dual-frequency wireless power transfer (DF-WPT) systems," *IET Microw. Antennas Propag.*, vol. 14, no. 7, pp. 617–628, 2020.

FILIPE FERREIRA received the B.Sc. degree in telecommunications engineering from the Federal University of Pampa (UNIPAMPA), Brazil, in 2017, and the M.Sc. degree in electrical engineering from the Federal University of Rio Grande do Sul (UFRGS), Porto Alegre, Brazil. His main research interests include communications and networks.

MAX FELDMAN received the B.Sc. and M.Sc. degrees in electrical engineering from the Federal University of Rio Grande do Sul (UFRGS), Porto Alegre, Brazil, in 2013 and 2020, respectively, where he is currently working toward the Ph.D. degree in networks and telecommunications. His main research interests include embedded systems, communication protocols, and industrial wireless networks.

GIOVANI BULLA received the B.Sc. degree in physics in 2004 and the Ph.D. degree in electrical engineering in 2010 from the Federal University of Rio Grande do Sul – UFRGS, Porto Alegre, Brazil, where he has been an Assistant Professor since 2016. His research interests include electromagnetic simulation, EMI/EMC, antenna design, RFID, and biological effects of RF.

VALNER BRUSAMARELLO received the B.E. degree in electrical engineering and the M.Sc. degree from the Universidade Federal do Rio Grande do Sul (UFRGS), Porto Alegre, Brazil, in 1992 and 1996, respectively, and the Ph.D. degree from the Universidade Federal de Santa Catarina, Florianópolis, Brazil, in 2000. He is currently a Professor with the department of Electrical Systems of Automation and Energy of UFRGS, Porto Alegre, Brazil. His main research interests include sensors and applied electronic instrumentation, digital signal processing, energy harvesting systems and wireless power transmission with more than 80 articles published in conferences proceedings, magazines, and scientific journals.

IVAN MÜLLER received the B.Sc., M.Sc., and Ph.D. degrees in electrical engineering from the Federal University of Rio Grande do Sul, Porto Alegre, Brazil. He has experience in Instrumentation, Computing, Electronics and Telecommunications, having researched on the following subjects: wireless sensor networks, industrial networks, communication protocols, and Eelectronics, with more than 90 articles published in conference proceedings, magazines, and journals.